Bull. Mater. Sci. (2024)47:2
https://doi.org/10.1007/s12034-023-03072-5

Real-time photothermal degradation of methylene blue dye by CuS thin film grown using a fully automated spray pyrolysis

SANTOSH K TRIPATHI*, PRAGATI MISHRA, SHAILENDRA KUMAR DWIVEDI, HIMANSHI CHAURASIA, ATENDRA S CHAUHAN, KAVITA AGARWAL and MAYANK DWIVEDI

Defence Materials and Stores Research and Development Establishment (DMSRDE), Kanpur 208013, India
*Author for correspondence (sktripathi23@gmail.com)

MS received 29 July 2022; accepted 16 July 2023

Abstract. The real-time photothermal degradation of methylene blue (MB) dye was studied using CuS thin film (TF) as a photocatalyst. The polycrystalline CuS TFs were fabricated on precleaned glass substrates by an aqueous solution of copper chloride and thiourea using a fully automated spray pyrolysis technique by varying temperatures (250–400°C). The properties of deposited films were studied by XRD, SEM, UV–Vis–NIR spectroscopy, photoluminescence (PL) and Hall measurement. XRD results show that the CuS TFs crystallized in the cubic phase with an average crystallite size ~22–30 nm. CuS TF grown at higher temperatures (350°C, 400°C) exhibited very low strain of about 0.55 and 1%, respectively. Hall study revealed that films deposited at 400°C had good electrical parameters with mobility (μ) of 0.866 $cm^2\ V^{-1}\ s^{-1}$, Carrier concentration (p) of 5.21 × 1019 cm^{-3} and conductivity (σ) of 49.4 Ω-cm^{-1}. The estimated optical bandgap of films were found to be in the range of 2.10–2.26 eV, revealing blue shift due to quantum size effects. The PL spectra showed two characteristic bands of the CuS films, at 422 nm and an intense green band at 504 nm. The copper sulphide TF showed high photocatalytic activities in a photo-decolourization of MB dye under irradiation of visible light, as CuS TF was able to completely decompose the dye in 160 min.

Keywords. CuS; automated spray pyrolysis; thin films; photoluminescence; photovoltaic materials; photocatalytic activity.

1. Introduction

Organic dyes are widely used in various industries such as textile, paper, plastic and chemical, being discharged into the environment, which can easily form highly toxic complexes by reacting with some metal ions present in wastewater to pollute water resources and triggering several problems [1,2]. This wastewater has highly harmful consequences on human health as well as the aquatic ecosystem, therefore it is essentially required to preserve before discharging into the running water. Oxidation of organic and biological molecules by photocatalysis is one of the most prominent techniques for minimizing the negative environmental effects of hazardous wastes and toxic pollutants [3,4].

The oxidative process of photocatalysis is based on the generation of electron–hole pairs in semiconductor materials by the absorption of photons, which can further generate free radicals, such as hydroxyl in the system to redox the compounds absorbed on the surface of a photocatalyst [2,5–7]. The natural and pollution-free resource of energy is sunlight, which possesses great potential in driving environmentally benign organic transformations [8]. The environmentally appealing fact is to energize photocatalyst materials by using solar irradiation, and this process is almost energy-self-sufficient and permits the design of a water treatment that is simple, robust and economical to set up and run [9]. The selection of materials for photocatalytic activity is the most important aspect. It is obvious that the semiconductors with suitable bandgap, flat band potential/energy levels and good adsorption properties in the visible region are most efficient for photocatalytic purposes because most of the solar energy falls in the visible region.

Metal sulphides have attracted extensive attention in recent years. Among these materials, copper chalcogenides reveal unique optical, electronic, physical and chemical properties with prospective and numerous applications as both the photocatalysis and the Fenton-like reactant [10–16]. Furthermore, the CuS-induced Fenton-like reactions are iron-free, resulting in the separation of reactants from ions and solid materials. The degradation of organic dye molecules in CuS-induced Fenton-like reactions can

Supplementary Information: The online version contains supplementary material at https://doi.org/10.1007/s12034-023-03072-5.

Published online: 16 December 2023

proceed efficiently without adjusting the pH value. These advantages make the CuS-induced Fenton-like reactions more cost-efficient by avoiding the ion removal and pH rectification. On the other hand, the elements S and Cu in the copper chalcogenides are 'liquidus' and can be used to fabricate other materials without destruction of morphology [17]. In order to obtain efficient charge separation and transportation, many copper chalcogenide nanostructures, such as nanospheres, nanodisks, flower-like and porous nanostructures and nanowires were designed with short charge diffusion length, high crystallinity and lower defects and studied their photocatalytic behaviour towards dyes [18–23]. However, very few reports have been published on the use of CuS thin films (TF) for photocatalytic studies [24–27]. The use of CuS TFs are advantageous in this study to avoid separation of catalyst from the mother solution and minimized secondary pollution.

Various synthesis methods, such as spray pyrolysis (SP) [28], chemical vapour deposition [29], sputtering [30], chemical bath deposition method [31], etc., are being used for the deposition of TFs. Among them, the SP technique is widely used on large scale for TF deposition on various glasses or conducting substrates due to its low cost, better reproducibility and easy handling. SP is a process in which a TF is deposited by spraying a solution on a heated substrate, where the constituents react to form a chemical compound. The reactants are chosen such that the products other than the desired compound volatilizes at the temperature of deposition. The main feature of SP technique is that it does not require high processing temperature, vacuum or sophisticated instrumentation, thus making large-area growth easier; this is of primary importance from the perspective of industrial-scale production.

Herein, we report a facile SP strategy to fabricate copper sulphide TFs. A cost-effective, fully automated SP technique was employed for the deposition of copper sulphide TFs on glass substrates using an aqueous solution of copper chloride and thiourea. The effect of growth temperatures on the properties of the deposited copper sulphide TFs was investigated. The evolution of the copper sulphide structure is described as well. The as-prepared CuS-nanostructured TFs exhibit unique light absorption performance and photocatalytic activity towards photodegradation of methylene blue (MB) dye.

2. Experimental

2.1 *Fabrication of CuS TFs and characterization*

The CuS TFs were grown using a non-vacuum fully automated SP technique, using copper chloride $CuCl_2{\cdot}2H_2O$ (Sigma Aldrich) and thiourea ($NH_2{\cdot}CS{\cdot}NH_2$, Merck) as a precursor for the spray solution. In a typical procedure, the aqueous solution of $CuCl_2{\cdot}2H_2O$ and thiourea in 1:1.5 molar ratios were used as precursor solution for the preparation of CuS TF. A quantity of 80 ml of the prepared aqueous solution was sprayed on a heated glass substrate, at a flow rate of 1.5 ml min^{-1} monitored by closely controlled SP (see schematic diagram in supplementary figure S1) throughout the experiment. The distance between the nozzle and the hot plate was maintained at 150 mm and air was used as a carrier gas at a pressure of 2 kg cm^{-2}. The CuS films were deposited at four different temperatures 250, 300, 350 and 400°C, labelled as P1, P2, P3 and P4, respectively. The prepared CuS TFs were thoroughly investigated. The structural properties and grain size of developed CuS TFs were studied using powder X-ray diffraction (PANalytical Xpert Pro) using CuKα (1.5406 Å). The bandgap energy of pyrolysed materials was studied by Ultra-violet Visible spectrosphotometer (Cery 5000). Surface morphology was studied by FESEM using Carl Zeiss Evo50 XVP Low Vacuum Scanning Electron Microscope along with an energy dispersive X-ray spectrometer (EDX). The thickness of the CuS TFs was measured using ZETA-388 KLA optical profilometer and found to be 1.8, 1.7, 1.4 and 1.2 μm for the samples P1, P2, P3 and P4, respectively.

2.2 *Photocatalytic process of CuS TF*

Methylene blue (MB), a common dye resistant to direct sunlight and biodegradation, was used as the degradation material to explore the catalytic behaviour of CuS TFs [32]. In a typical reaction setup, CuS (P4) TF (2 × 2 cm) was fixed in a 100 ml beaker containing 100 μl MB in 50 ml DDI water and 100 μl of H_2O_2 was added into it and the reaction system was kept at 25°C. The mixture was stirred at 250 rpm in the dark for 10 min to establish the adsorption–desorption equilibrium between the CuS TFs and MB molecules. The mixture was then illuminated by direct 60 W bulb fixed at 10 cm distance from the reaction vessel, to perform the photocatalytic reaction. During the process, a 2 ml aliquot of the mixture was taken out in every 10-min intervals to determine MB concentrations. In addition, 2 ml aliquots were also taken before and after mixing in the dark to investigate variations in MB concentration. The changes in MB concentration were monitored by the UV–Vis absorption intensities of the light irradiated sample at every 10-min time interval. A schematic setup of the experiment was illustrated in figure 1. Similar experiments were carried out without controlling the temperature. In this case, the real temperature of the reaction was raised upto 42°C. Hence thermal-induced photocatalytic behaviour was monitored and compared with photocatalytic behaviour at normal temperature.

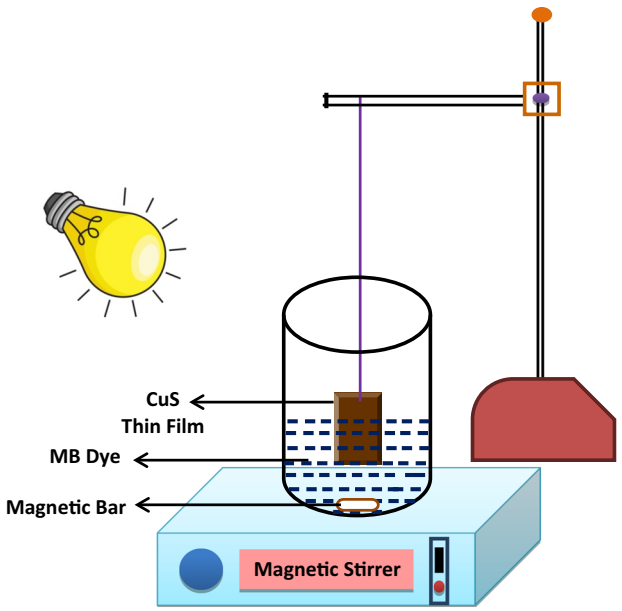

Figure 1. Schematic diagram of experimental set up for photocatalytic activity.

3. Results and discussion

3.1 *Structural properties*

The structural properties of sprayed TFs were characterized using XRD. Figure 2 displays XRD patterns of CuS TFs deposited at different temperatures. The film deposited at 250 and 300°C were amorphous in nature, whereas the films deposited at 350 and 400°C showed well-defined peaks at 2θ values of 28.34, 32.98, 46.91 and 56.36° corresponding to the lattice planes (111), (200), (220) and (311), respectively. The XRD patterns revealed that the deposited CuS TFs are polycrystalline in nature with a cubic structure

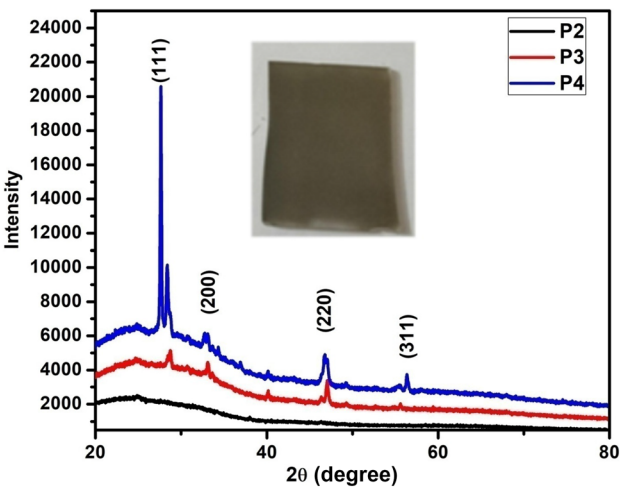

Figure 2. XRD patterns of CuS thin films deposited at various growth temperatures and actual photograph of sprayed CuS thin film (inset).

[JCPDS 65-2980] [33]. It can be observed that the crystallinity of deposited films increased with increasing growth/annealing temperatures. Hence it can be concluded from the XRD results that 400°C is the optimum growth temperature for the deposition of good crystalline CuS TFs. The Scherrer's formula was used to evaluate the crystallite size of CuS nanostructure. The obtained crystallite size of the deposited films is summarized in table 1.

The properties of CuS films depend significantly on the microstructure of the films, as well as on the residual stress that occurs due to thermal and/or lattice mismatch between the film and substrate. Therefore, the measurement of residual strain in CuS TFs is important to predict the performance of electronic devices fabricated out of it. In this study, the residual strain is determined by XRD. The residual strain produced in the samples was calculated using the Williamson–Hall (W–H) equation [34].

$$\beta\cos\theta/\lambda = K/D + 4\varepsilon\sin\theta/\lambda \quad (1)$$

where β is the full-width at half-maximum of XRD peak, K is a constant, D is the size of the crystallite, ε is the strain and λ is the X-ray wavelength (0.154 nm). To calculate the residual strain produced in the TFs, a graph of $\beta\cos\theta/\lambda$ *vs.* $\sin\theta/\lambda$ was plotted for the films deposited at temperatures (350 and 400°C). Each graph shows a straight line where the slope of the straight line gives the value of residual strain in the samples. The slope could be either negative or positive depending on the type of strain. The negative slope is associated with compressive strain, whereas a positive slope indicates tensile strain. It can be noted from the W–H plots (supplementary figure S2) that the strain produced in the films (P3, P4) is tensile. The percentage of residual strain was found to be very low as compared to earlier reported values of strain for CuS [35]. A dense and crack-free CuS TF with minimum strain can be fabricated by controlling the flow rate of the precursor solution and maintaining the appropriate gap between the substrate and the nozzle. It has been reported that a slow flow rate and a larger gap between nozzle and substrate will result in dense, low strained and crack-free morphology of TF [36]. It is obvious that the higher the flow rate, the larger will be the size of droplets coming from the nozzle; these will accumulate in large amounts over the substrate and will take a longer time to dry, which leads to the formation of porous and cracked CuS TF. Our results suggest that the controlled low flow rate, the height of spray nozzle from the substrate, and the temperature play a key role in the fabrication of high-quality defect/strain-free CuS TF at low cost.

3.2 *Morphological properties*

Figure 3a shows an SEM micrograph of as-deposited CuS TF. The film deposited at 250°C shows a non-uniform distribution of particles having different shapes and sizes. Nano-rod-like morphology was seen in the film deposited at

Table 1. Crystallite size and thickness of CuS thin films deposited at different temperatures.

Deposition temperature (°C)	FWHM (degree)	Crystallite size (nm)	Thickness (μm)
250	...	Amorphous	1.8
300	...	Amorphous	1.7
350	0.36	22.35	1.4
400	0.27	29.48	1.2

300°C (see figure 3b). However, CuS TF grown at 350°C shows dense morphology with a uniform distribution of particles over the substrate (see figure 3c). As the annealing temperature rises to 400°C, a flower-like morphology can be seen covering the entire substrate (see figure 3d).

The EDAX was used to analyse the chemical composition of copper sulphide (CuS) TFs. As shown in supplementary figure S3, the EDAX spectrum of the copper sulphide TF deposited at 400°C onto the glass substrate. The average atomic ratio of Cu:S was found to be 11.64:11.87, showing an excellent stoichiometry (Cu/S: 0.94:1) in the prepared CuS film. Furthermore, other peaks corresponding to Si, O and C were also observed, which is related to their presence in the glass substrate. Therefore, on the basis of the EDX and XRD data, the composition of the film could be confirmed as CuS without other mixed phases.

The surface morphology and crystalline nature of synthesized TFs were also analysed by the HRTEM and SAED pattern. Figure 4 shows the HRTEM images and SAED pattern of representative CuS TF deposited by pyrolysis of precursor solution at 400°C. It clearly shows the formation of compact aggregated nanopetal-like morphology. It indicates that the good crystalline nature of TF with lattice fringes d-spacing of 2.9 Å (figure 4c) corresponding to (211) plan of CuS and 3.040 Å (figure 4d) correspond to d (102) reflections plans [37–39]. Further the SAED pattern in figure 4b shows the formation of a distinct ring pattern with dots, which confirms the polycrystalline nature of synthesized materials. The HRTEM and SAED patterns study reveals that the synthesized CuS TF is well in accordance with the XRD pattern.

3.3 *Optical properties*

In order to investigate the optical properties of sprayed CuS TFs, absorbance was recorded using a Varian carry-5000UV-Vis-NIR spectrophotometer in the wavelength ranging from 300 to 1200 nm. The absorption spectra (supplementary figure S4a) show CuS TFs deposited at various growth temperatures (250, 300, 350 and 400°C). Blue shifting with increasing growth temperatures can be seen in the absorption spectra of CuS TFs.

The optical bandgap (E_g) was calculated by Tauc relation:

$$(\alpha hv) = \mathrm{A}(hv - E_g)^n \quad (2)$$

where α is the optical absorption coefficient, A is a constant, and n depends on the transition type. The optical bandgap values of CuS TFs were calculated by extrapolating $(\alpha hv)^2$ plot against photon energy (hv), as shown in supplementary figure S4b. The optical bandgaps of CuS TFs fabricated at

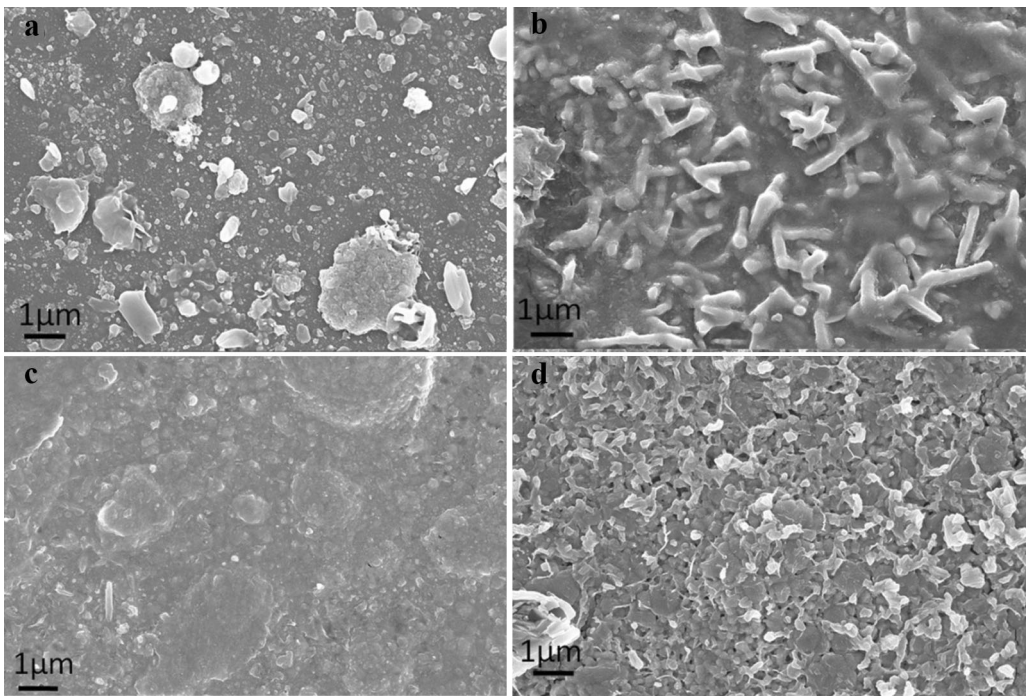

Figure 3. (**a**) SEM micrograph of CuS thin film deposited at 250, (**b**) 300, (**c**) 350 and (**d**) 400°C.

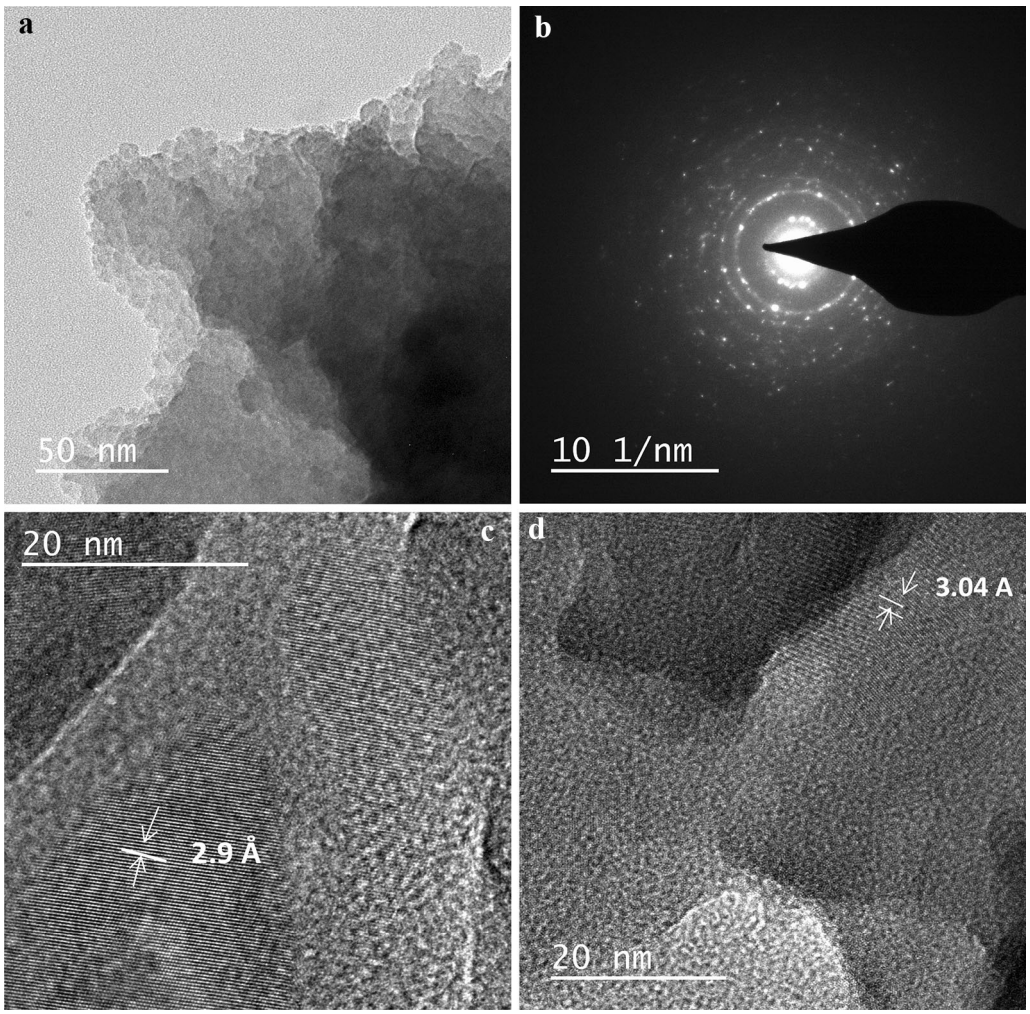

Figure 4. HRTEM and SAED patterns of CuS thin film deposited at 400°C.

various temperatures are tabulated in table 2. It is clear from table 2 that there is a slight shift in bandgap energy (∼0.10–0.15 eV) towards lower wavelength (higher energy) as we increase the deposition temperature compared to bulk covellite CuS (∼2.2 eV) [40,41]. This shift in bandgaps is probably due to the quantum confinement effects, i.e., the CuS crystals present in the TFs matrix behave as three-dimensionally confined structures [42]. Furthermore, the average diameters of the nanocrystallites in the films are in the range of 22–30 nm estimated on the basis of XRD line broadening.

Table 2. Calculated bandgap using Tauc relation for CuS thin films.

Growth temperature (°C)	Bandgap (eV)
250	2.26
300	2.20
350	2.20
400	2.10

Photoluminescence (PL) study was carried out for all the samples in the wavelength ranging from 350 to 600 nm using xenon lamp with excitation of 350 nm. Supplementary figure S5 displays PL spectra of the CuS TFs. The film deposited at 250°C (P1) shows two broad peaks, e.g., one at 392 nm and other at 500 nm. The broad emission band at 392 nm is attributed to copper-thiourea precursor. As the growth temperature increases from 250°C, [300(P2), 350(P3), 400°C(P4)] a new shoulder started at about 422 nm, which may be attributed to the band-to-band transition and corresponds to the room temperature bandgap energy of about 2.9 eV for the CuS polycrystalline films. In addition to that, there is a wide green emission band together with an apparent peak around 504 nm (∼2.5 eV) close to the effective bandgaps of these materials (table 2), mainly attributed due to the radiative recombination between the conduction band (CB) and the widespread copper-vacancy-related acceptor levels around the valence band (VB) edge [25]. However, the blue shift of 12–15 nm

also seen in emission peaks towards the higher wavelength region could be considered as a sign of the quantum confined effect due to the formation of the nano-sized CuS crystals on the surface, shown in figure 3.

3.4 *Electrical properties*

In order to evaluate the electrical conductivity, type of conductivity, mobility and carrier concentration, the films were characterized by Hall measurement at 20°C using the Van der Pauw method. The Hall-mobility of the TFs was determined by measuring the change in resistance (ΔR) and the magnetic field (ΔB), which was applied perpendicular to the thickness (t) of the sample. Hall-mobility μ is given by the relation:

$$\mu = \frac{t}{\Delta B} \cdot \frac{\Delta R}{\rho} \tag{3}$$

where ρ is room temperature resistivity of the sample. The carrier concentrate on (p) was calculated using the formula,

$$\text{Carrier concentration } p = \frac{1}{R.\rho} \tag{4}$$

The Hall measurement was carried out on CuS TFs deposited by SP technique. Hall measurements show that, as expected, all the CuS films have had p-type conductivity. The mobility (μ), conductivity (σ) and carrier concentration (nc) of CuS TF deposited at 250°C was found to be 0.177 $cm^2\ V^{-1}\ s^{-1}$, 7.86 $\Omega\text{-}cm^{-1}$ and 1.89 × 1017 cm^{-3}. Results show that the film grown at 250°C is more resistive due to poor carrier concentration present in the sample. As the deposition temperature increased from 300 to 350°C, the mobility slightly decreased to 0.523 $cm^2\ V^{-1}\ s^{-1}$, carrier concentration increased to 3.55 × 1019 cm^{-3} and the conductivity was found to be 24.6 $\Omega\text{-}cm^{-1}$. CuS TF deposited at 400°C exhibits improved electrical parameters with mobility of 0.866 $cm^2\ V^{-1}\ S^{-1}$, carrier concentration 5.21 × 1019 cm^{-3} and conductivity of 49.4 $\Omega\text{-}cm^{-1}$. In our case, the obtained values of hole concentration (p) and mobility (μ) were found to be in the range 1017–1019 cm^{-3} and 0.523–0.866 $cm^2\ V^{-1}\ s^{-1}$, respectively, which are higher than those obtained for CuS TFs deposited via dip coating and chemical bath deposition techniques [25,43]. Results demonstrated that automated SP techniques could be a better solution to fabricate large-scale good quality and conducting CuS TFs for solar cell application. Supplementary figure S6 displays the variation of conductivity and thickness of CuS TF as a function of growth temperature. From the graph, it is observed that the conductivity of CuS TFs tends to increase with increasing growth temperature. The p, μ and σ values of the CuS TFs are tabulated in table 3.

3.5 *Photocatalytic activity of the CuS TF*

3.5a *Photocatalytic activity of CuS TF at room temperature:* The photocatalytic behaviour of optimized CuS(P4) TF was studied for the degradation of MB dye under irradiation of light in the presence of H_2O_2. The reaction system as shown in figure 1 was first kept in dark for 10 min to generate adsorption desorption equilibrium between CuS TFs and MB molecules. After that light (60 W bulb) was turned on to irradiate the sample and degradation of MB was monitored by UV–Vis spectroscopy. A UV–Vis spectrum of MB shows two characteristic absorption peaks 614 and 662 nm. According to Lambert beer law, the concentration of MB is directly proportional to the intensity of the characteristic absorption peak [44]. Hence the change in absorption peak at 662 nm was used to evaluate the catalytic performance. The MB degradation was expressed by plotting (C_t/C_0) as a function of irradiated time t, where C_t/C_0 is the concentration of MB at time t and 0, respectively, and was replaced by the absorption intensities for the purpose of calculation. UV–Vis spectra shown in figure 5a clearly show that there is no change in absorption intensity during the first 10 min when the reaction system is kept in the dark. After that the intensity of MB absorption decreased gradually upon increasing the irradiation time. This is because of the generation of the free carriers by the irradiation of light that promotes the fast degradation of MB and it was observed that the 10% of MB concentration reduced after 30 min exposure to light indicating good catalytic performance.

Langmuir-Hinshelwood first-order-reaction model [45] used to study the photocatalysis kinetics of a semiconductor:

$$\ln(C_0/C_t) = kt \tag{5}$$

where C_t and C_0 are as defined above, k is the photodegradation rate constant, and t is the solar irradiation time. Equation (5) affords the photodegradation rate constant k through a plot of $\ln(C_0/C_t)$ *vs.* solar irradiation time t. Figure 5c illustrates the dependency of $\ln(C_0/C_t)$ on time, and the line of best-fit yields k from its slope. The calculated k and coefficient of determination (R^2) are 0.0061 min^{-1} and 0.987, respectively.

3.5b *Effect of temperature on photocatalytic activity of CuS TF:* In the second part of our experiment we conducted the above photodegradation experiment in real-time measurement means without maintaining the room temperature reaction system. It is obvious to study this because local heat is generated during the exposure of reaction system by light. Hence the effect of the temperature on the photocatalytic process needs to be established to study the real-time photodegradation behaviour of MB dye. That is why we have performed the same experiment without cooling of reaction system and measured the UV–Vis spectra with irradiation time and temperature as shown in figure 6a. The decrease of absorption peak seen in UV–Vis spectra with increasing the light exposure time and it was observed that the absorption peak of MB almost disappeared within 150 (total

Table 3. Electrical parameters obtained from Hall's study for CuS thin films.

Deposition temperature (°C)	Mobility, μ (cm^2/V^{-1} S^{-1})	Carrier concentration p (cm^{-3})	Conductivity $\sigma(\Omega\text{-cm})^{-1}$)
250	0.177	1.89×10^{17}	7.86
300	0.681	2.99×10^{18}	34.2
350	0.523	3.55×10^{19}	24.6
400	0.866	5.21×10^{19}	49.4

160) min. Figure 6b shows the MB degradation dynamics with photothermal conversion. It is worth noting that we have performed the photocatalysis process under the real-time conditions of sample, in which heat is generated locally during the exposure of light and it reaches upto 42°C. Figure 5c displayed the photographic images of the exposed MB solution at various time intervals.

The rate constant k of photodegradation was calculated by the plot of $\ln(C_0/C_t)$ *vs.* irradiation time t, as depicted in figure 6d. The value of k and coefficient of determination (R_2) obtained in this manner was 0.025 min^{-1} and 0.954, respectively. Compared to the photodegradation rate constant obtained at room temperature (25°C) ($k = 0.0061$ min^{-1}), the photothermal-assisted reaction provides an enhancement of photodegradation rate of ~309.8% ((0.025–0.0061)/0.0061 = 309.8%). Figure 6d shows that the relationship between $\ln(C_0/C_t)$ and solar irradiation time t is not linear, as it was remained at 25°C for the reaction system, and the slope appears to have progressively increased. The real-time photodegradation rate k increased from $k_1 = 0.0025$ (during the first 10 min of photodegradation) to $k_2 = 0.00437$ (during the second 10 min) to $k_3 = 0.0169$ (during the third 10 min). This observed phenomenon is most likely caused by the spontaneous temperature rise due to irradiation of the reaction system, as shown in figure 6d. The thermocouple recorded a nearly uniform temperature since the mixture

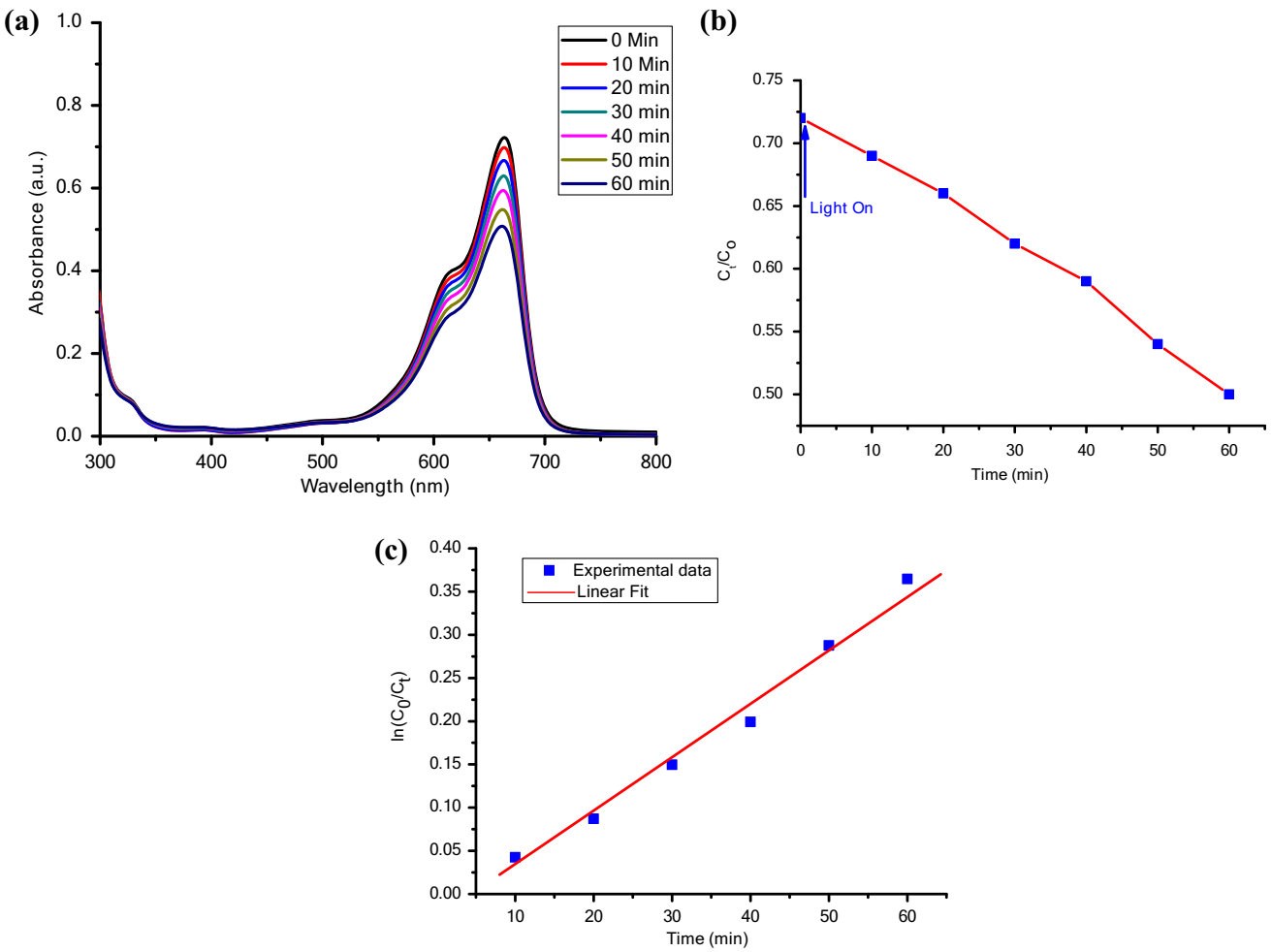

Figure 5. Photocatalytic activity of the CuS thin film at 25°C. (**a**) Time dependence of the UV–vis absorption spectrum of the MB dye. (**b**) Plot of C_t/C_0 *vs.* time and (**c**) plot of $\ln(C_0/C_t)$ *vs.* irradiation time.

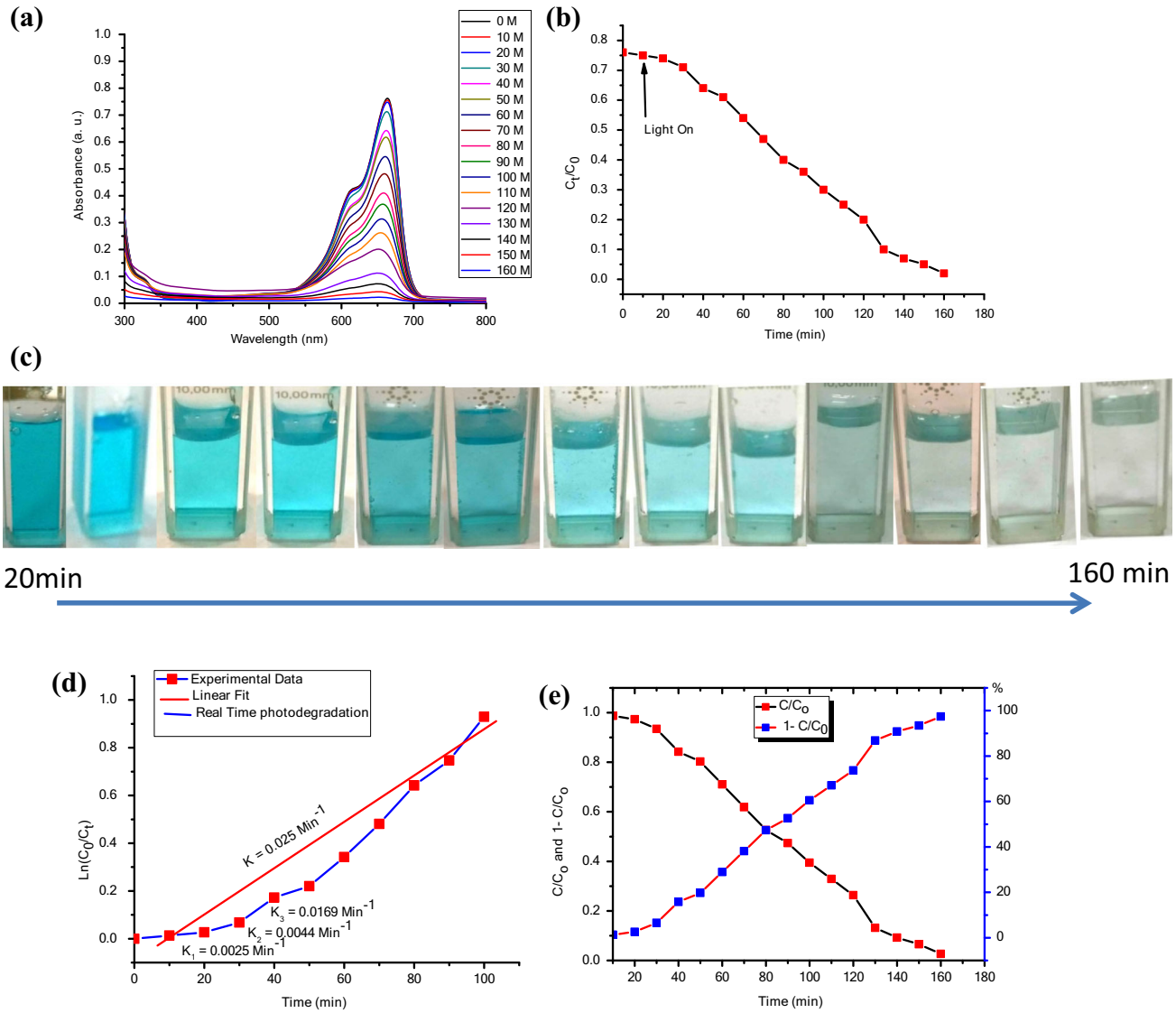

Figure 6. Photocatalytic thermal activity of the CuS thin film at 42°C. (**a**) Time dependence of the UV–vis absorption spectrum of the MB dye. (**b**) Plot of C_t/C_0 *vs.* time. (**c**) Colour of sample with respect to irradiation time. (**d**) Plot of $\ln(C_0/C_t)$ *vs.* irradiation time and (**e**) plot of C_t/C_0 and $1–C_t/C_0$ *vs.* time.

was stirred during the experiment. During photocatalysis, the temperature of the water-cooled reaction system was kept at 25°C, while the temperature of the uncooled reaction system was raised from 25 to 42°C over the course of the exposure of light.

Figure 6e shows the evaluation of photodegradation of MB as a function of irradiation time in the presence of CuS TF under visible light. The photodegradation of MB was monitored as the normalized range in its concentration and also using degradation efficiency. The intersection of these two curves (C/C_o and $1–C/C_o$) shows the half-life of MB, which is the time taken for the concentration of MB to decrease by half. From the figure, it has been noticed that the intensity of the absorption peaks corresponding to MB in the presence of CuS TF decreased gradually upon increase in exposure time, thereby the concentration of MB reaches its half after 80 min (half-life). The degradation efficiency for CuS TF has reached ∼98% after 160 min.

3.5c *Mechanism of photocatalysis in uncooled photodegradation process:* The CuS TF is largely comprised of many unfolded nanocrystallites that absorb photons and form electron–hole pairs when exposed to light. Furthermore, its hierarchical structure allows for multiple scattering of solar light, resulting in better photo absorption. The photodegradation of MB was carried out in the presence of H_2O_2 which not only react with CuS but also accept photogenerated electron produced by CuS under visible-light irradiation. Hence H_2O_2 inhibits electron–hole

pair recombination, which further enhances the production of reactive species such as OH radical and enhances visible–light-induced photocatalysis.

In a photochemical reaction, the photoinduced electrons and holes are generated as a result of the excitation of electrons from VB to CB upon visible-light illumination. The level of the VB and the CB of CuS has been calculated using the given relation [46].

$$E_{VB} = X - E_e + 0.5E_g \quad (6)$$

$$E_{CB} = E_{VB} - E_g \quad (7)$$

In equations (6 and 7), E_{VB} is the VB potential edge, X is the electronegativity of the semiconductor material, E_e is the free electron energy on the hydrogen scale ($\sim$4.5 eV), E_g is the energy bandgap of the prepared CuS TF catalyst (2.10 eV calculated from UV–Vis result)), and E_{CB} is the CB potential edge. The electronegativity of the CuS material can be obtained from the arithmetic mean of the electron affinity and the first ionization energy of the constituent atoms, as reported in the literature to be 5.29 eV. The calculated CB and VB potentials of CuS TF catalyst are -0.26 and 1.84 eV *vs.* normal hydrogen electrode, respectively. A corresponding band diagram of CuS TF has been plotted and shown in figure 8, which indicates that the photogenerated electron and hole can stimulate both the adsorbed oxygen and water molecules on the catalyst surface to produce reactive oxygen species such as $\bullet O_2^-$ (superoxide anion) and •OH (hydroxyl) radicals, respectively. These reactive oxygen species can initialize the catalytic reactions by typical reaction pathways on the catalyst surface to degrade the MB molecules [47,48].

These reactive species are used to better understand the possible photocatalytic mechanism for the degradation of MB dye. In an aqueous medium, the photocatalyst under the light irradiation produces different reactive species such as superoxide, holes and hydroxyl radicals, which are responsible for the photodegradation of organic contaminants. To understand the specific roles of these reactive species, the controlled experiments were performed employing different scavengers such as disodium ethylene diamine tetraacetic acid (Na_2EDTA) as surface generated holes (h^+), isopropyl alcohol (IPA) for the hydroxyl radicals (•OH), and p-benzoquinone (pBQ), as superoxide radical ($\bullet O^{2-}$) trapping, and the results are depicted in figure 7a and b. The more the MB dye degradation rate is suppressed by the addition of one scavenger, the more important role it plays in the photodegradation process by the corresponding active species. Previous literature showed that small aliphatic alcohols such as methanol, ethanol, isopropyl alcohol and tertiary butyl alcohols could be employed as hydroxyl radical scavengers to investigate the role of hydroxyl radicals in the photocatalytic degradation of dyes. These aliphatic alcohols produce some intermediate products with high inertness during light irradiation, in that way inhibiting the reaction between the hydroxyl radicals and dye molecules [46,49,50]. In this study, we have taken IPA as a scavenger for the hydroxyl radical. It was observed that in the presence of IPA, the MB dye degradation decreased from 96.6 to 49.7.3% (figure 7c), demonstrating that the hydroxyl radicals (•OH) play a major role in the degradation process. Furthermore, pBQ is a good agent for the tapping of superoxide radicals ($\bullet O^{2-}$); while adding pBQ to the reaction, the degradation rate comes down to 92.7%. On the other hand, Na_2EDTA has been added as a hole-trapping agent. It is well-known that it can be easily oxidized and irreversibly decomposed into glyoxylic acid and ethylene diamine *N*,*N*′-diacetic acid [36,37,50]. After the addition of Na_2EDTA, the degradation rates of MB dye decreased from 96.6 to 74.3%. This confirms that the photogenerated hydroxyl radicals were one of the primary active species and holes that produce superoxide ($\bullet O^{2-}$) were a secondary active species for the degradation of MB dye with the CuS TF photocatalysts.

Considering the above observation, the plausible photocatalytic mechanism and the pathways for the MB dye degradation in the presence of CuS photocatalyst are shown in figure 8. The photoexcitation of electrons from the electrons leads to charge separation followed by charge transfer to the edge-active sites. As a result, CuS TF shows superior photocatalytic efficiency. The photocatalytic degradation using CuS TF catalyst is given by the following equations (8–13). In this mechanism, first H_2O_2 molecules react with Cu^+ ions and produce $OH^\bullet$ radicals. These $OH^\bullet$ radicals then react with MB molecules and produce free radicals, which oxidized in the presence of oxygen to produce degraded or mineralized products [43,51].

$$Cu^{2+} + H_2O_2 \rightarrow H^+ + CuOOH^+ \quad (8)$$

$$CuOOH^+ \rightarrow HOO^\bullet + Cu^+ \quad (9)$$

$$2HOO^\cdot \rightarrow 2OH^\bullet + O_2 \quad (10)$$

$$Cu^+ + H_2O_2 \rightarrow Cu^{2+} + OH^\bullet + OH^- \quad (11)$$

$$RH + OH^\bullet \rightarrow R^\bullet + H_2O \quad (12)$$

$$R^\bullet + O_2 \rightarrow \text{degraded or mineralized products} \quad (13)$$

where R is the MB molecule.

In the photocatalytic process, photothermal conversion has a significant impact on catalysis performance. During the photothermally induced photocatalysis process, CuS nanocrystallites react as photothermal conversion medium and photocatalyst simultaneously. Consequently, the separation and transfer of the photogenerated carriers is critical in the photocatalytic process [23]. Figure 8 illustrates the most probable mechanism of photothermal conversion to improve the photodegradation of MB. There are three major factors that affect the photothermal degradation process, Firstly, the mobility of the carriers in the crystallites may affect by increasing temperature, as the carriers are normally transported faster at high temperatures [52]. As a result, enhanced carrier mobility may be the most important factor in boosting the photocatalytic activity of the CuS TF.

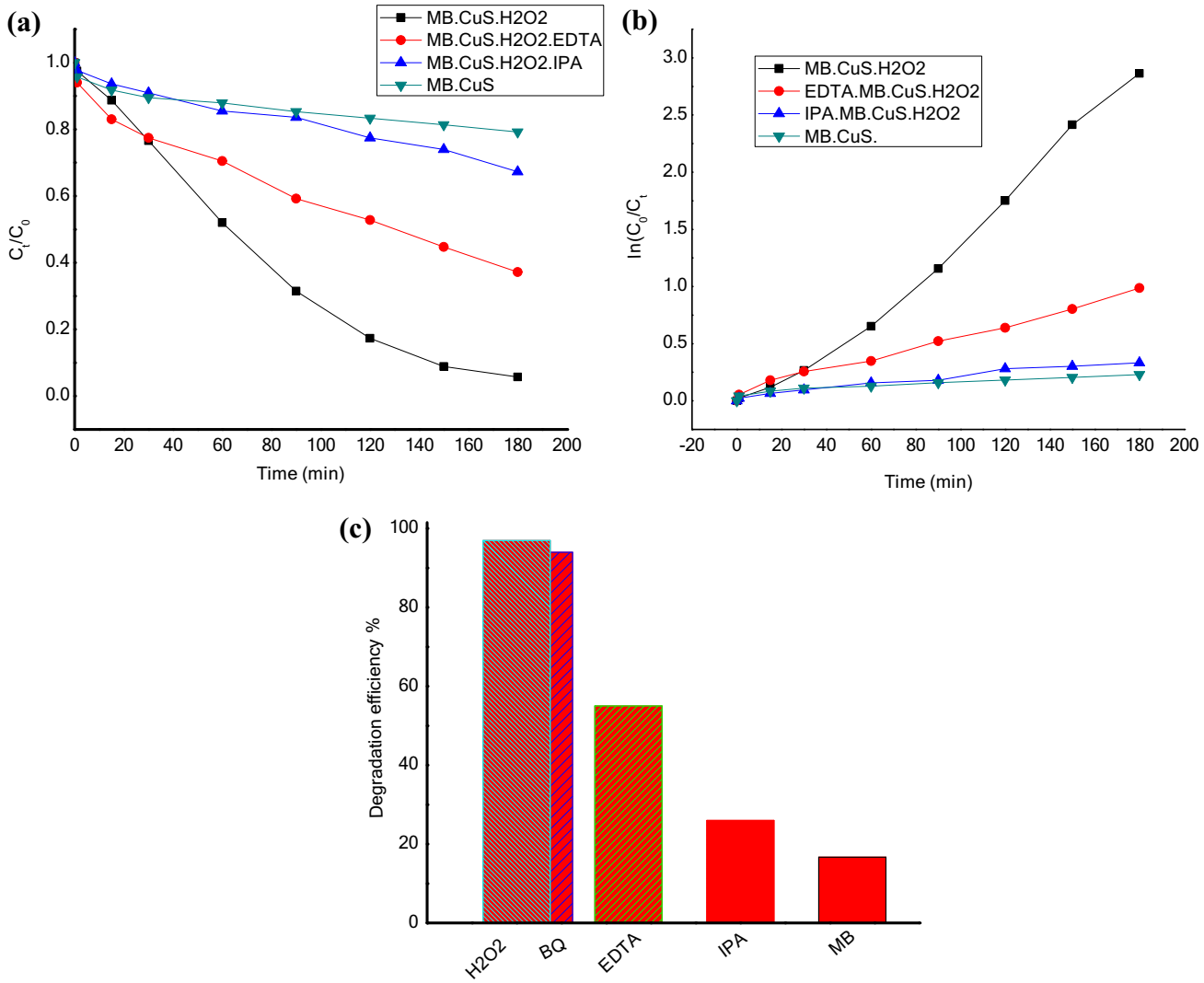

Figure 7. Photothermal induced photocatalytic degradation of the MB dye in the presence of various scavengers. (**a**) Plot of C_t/C_0 *vs.* time. (**b**) Plot of $\ln(C_0/C_t)$ *vs.* irradiation time. (**c**) Percent degradation of MB in the presence of scavengers**.**

Secondly, the photoexcitation efficiency of CuS TF increases with an increase of temperature, which leads to boost up the photocatalytic performance. The photoinduced carrier rate G is calculated as $G = \alpha(\hbar\omega)\mathrm{J}/\omega$, where $\alpha(\hbar\omega)$ is the optical absorption coefficient and J is the constant optical power density [53]. Photons with energies greater than the bandgap (E_g) between the VB and CB can be absorbed for direct photoenergy transition, whereas photons with energies lesser than E_g are involved in indirect transitions, and the process is temperature-driven. Hence, indirect transitions have a much smaller effect than direct transitions. Consequently, photothermal conversion may have an insignificant effect on the photoexcitation efficiency of CuS catalysts.

Thirdly the degradation of MB is an endothermic process; hence increases in the reaction temperature may affect the rate of photodegradation of MB. The rate of reaction could be calculated by Arrhenius's empirical equation [54]: Rate = $A\ \exp(-E_o/RT)$; where A is the pre-exponential factor, E_a is the apparent activation energy, T is the reaction temperature. Generally, the apparent activation energy is not very high for the photooxidative decomposition of MB; therefore, the reaction rate would increase with increasing the reaction temperature [55]. Furthermore, due to localized solar heat, a temperature gradient would form on the surface of the CuS TF, which would facilitate the diffusion of reactions and products [47]. Hence, the localized solar-thermal conversion effect on CuS enables faster degradation and faster release of kinetics [56].

4. Conclusion

We have demonstrated the fabrication of low-strain polycrystalline CuS TFs by fully automated SP technique by controlling the flow rate, temperature and height of the nozzle above the substrate. The deposition parameters were optimized to obtain crack-free uniform CuS TFs by varying

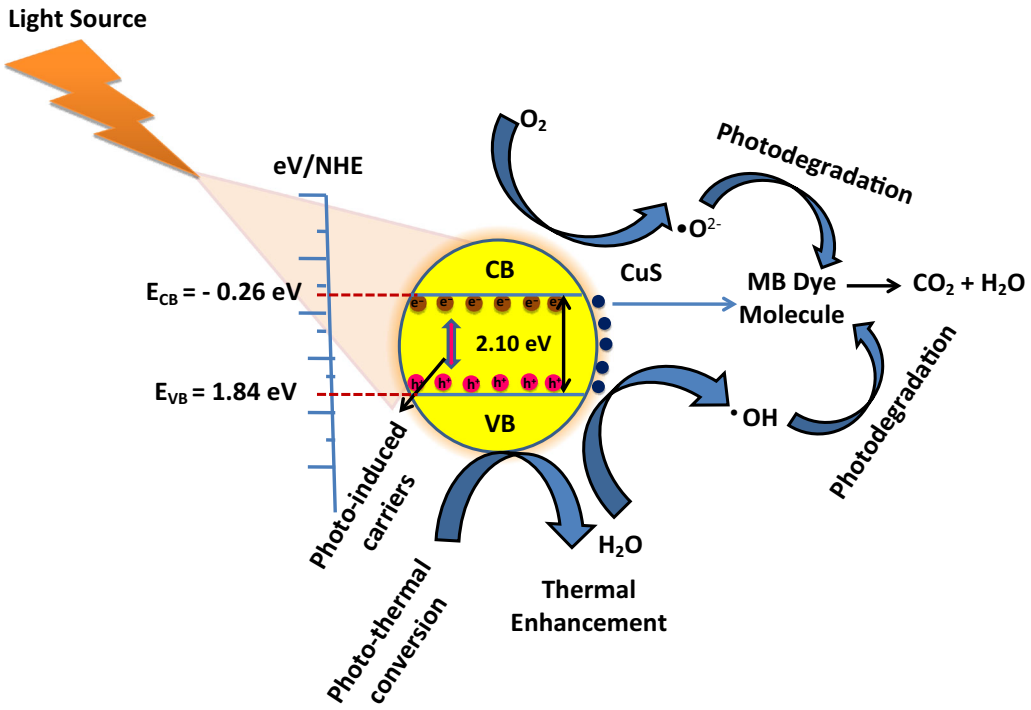

Figure 8. Band diagram of CuS TF and mechanism of photocatalytic degradation of MB dye.

deposition temperatures (250–400°C). XRD results show that the films deposited at 350–400°C were crystallized in the cubic phase with an average crystallite size ∼22–30 nm. Hall's study demonstrated that film grown at 400°C has good electrical properties. The PL spectra revealed not only the direct nature of the bandgap energy and the presence of widespread acceptor-like copper-vacancy levels around the VB edge tends to reduce the bandgap, but also the blue shift around 504 nm is attributed to the quantum confinement effect due to the formation of nanosized CuS crystals on the surface. The flow rate of precursors and temperature play a crucial role in the deposition of high-quality CuS TFs, which is beneficial for photo-absorbing layers in thin-film photocatalysts in a cost-effective manner. The photocatalytic activity of CuS TF for photodegradation of MB shows that the thermal-induced photodegradation rate enhanced by 309.8 times faster than normal temperature. Moreover, the concentration of MB reaches half after 80 min of irradiation. Hence CuS TFs may play a vital role in the design of catalysts for the clean and efficient harvesting of solar energy for photocatalysis without imposing any secondary environmental hazards.

Acknowledgement

We gratefully acknowledge the continuous support from the Director, DMSRDE, and for his permission to publish this work. This work was funded by the Defence Research and Development Organization (DRDO), Ministry of Defence, Government of India, New Delhi (Project No. DRM-559). We thank the Department of Chemical Engineering of Banasthali Vidyapeeth, Rajasthan, for providing support to Pragati Mishra to complete her short project at DMSRDE, Kanpur. Help received from Mr R D Verma, Mr Dilip K Saha, Ram Sobit Saha and members of CAF Division, DMSRDE, Kanpur, during the experiments is very much appreciated. Thanks are due to IIT, Kanpur, for UV–Vis and TGA, SEM and XRD characterization.

References

[1] Sharma M, Jain T, Singh S and Pandey O P 2012 *Sol. Energy* **86** 626
[2] Wang C, Ao Y, Wang P, Zhang S, Qian J and Hou J 2010 *Appl. Surf.* **236** 4125
[3] He T, Ma H, Zhou Z, Xu W, Ren F and Shi Z 2009 *Polym. Degrad. Stabil.* **94** 2251
[4] Wang X, Liu G, Lu G Q and Cheng H M 2010 *Int. J. Hydrogen Energ.* **35** 8199
[5] Andrade G R S, Nascimento C C, Neves E C, Barbosa C D A E S, Costa L P and Barreto L S 2012 *J. Hazard. Mater.* **203–204** 151
[6] Li Y, He X and Cao M 2008 *Mater. Res. Bull.* **43** 3100
[7] Vineetha M N, Matheswaran M and Sheeba K N 2012 *Sol. Energy* **91** 368
[8] Lang X, Chen X and Zhao J 2014 *Chem. Soc. Rev.* **43** 473
[9] Janin T, Goetz V, Brosillon S and Plantard G 2013 *Sol. Energ.* **87** 127

[10] He W, Jia H, Xi L, Lei Y, Li J, Zhao H *et al* 2012 *Nanoscale* **4** 3501

[11] Feng X, Li Y, Liu H, Li Y, Cui S, Wang N *et al* 2007 *Nanotechnology* **18** 145706

[12] Cheng Z, Wang S, Wang Q and Geng B 2010 *Cryst. Eng. Commun.* **12** 144

[13] Zhu T, Xia B, Zhou L and Lou X W 2012 *J. Mater. Chem.* **22** 7851

[14] Wu C, Yu S H, Chen S, Liu G and Liu B 2006 *J. Mater. Chem.* **16** 3326

[15] Cao H, Qian X, Wang C, Ma X, Yin J and Zhu Z 2005 *J. Am. Chem. Soc.* **127** 16024

[16] Tanveer M, Cao C, Ali Z, Aslam I, Idrees F, Khan W S *et al* 2014 *Cryst. Eng. Commun.* **16** 5290

[17] Zhuang T T, Fan F J, Gong M and andYu S H, 2012 *Chem. Commun.* **48** 9762

[18] Freymeyer N J, Cunningham P D, Jones E C, Golden B J, Wiltrout A M and Plass K E 2013 *Cryst. Growth Des.* **13** 4059

[19] Wei T, Liu Y, Dong W, Zhang Y, Huang C, Sun Y *et al* 2013 *ACS Appl. Mater. Inter.* **5** 10473

[20] Zhao Y, Pan H, Lou Y, Qiu X, Zhu J J and Burda C 2009 *J. Am. Chem. Soc.* **131** 4253

[21] Zhang F and Wong S S 2009 *Chem. Mater.* **21** 4541

[22] Shawky A, El-Sheikh S M, Gaber A, El-Hout S I, El-Sherbiny I M and Ahmed A I 2020 *Appl. Nanosci.* **10** 2153

[23] Wang X, He Y, Hu Y, Jin G, Jiang B and Huang Y 2018 *Sol. Energy* **170** 586

[24] He Y B, Politya A, Osterreicher I, Psterer D, Gregor R, Meyer B K *et al* 2001 *Physica B* **308–310** 1069

[25] Adelifard M, Eshghi H and Mohagheghi M M 2012 *Appl. Surf. Sci.* **258** 5733

[26] Nomura R, Miyawaki K, Toyosaki T and Matsuda H 1996 *Chem. Vap. Dep.* **2** 174

[27] Schneider S, Yang Y and Marks T J 2005 *Chem. Mater.* **17** 4286

[28] Isac L, Duta A, Kriza A, Enesca I A and Nanu M 2007 *J. Phys.: Conf. Series* **61** 477

[29] Schneider S, Ireland R, Hersam M C and Marks T J 2007 *Chem. Mater.* **19** 2780

[30] Yamamoto Y, Yamaguchi T, Tanaka T, Tanahashi N and Yoshida A 1997 *Sol. Energy Mater.* **49** 399

[31] Mukherjee N, Sinha A, Khan G G, Chandra D, Bhaumik A and Mondal A 2011 *Mater. Res. Bull.* **46** 6

[32] Shu Q W, Lan J, Gao M X, Wang J and Huang C Z 2015 *Cryst. Eng. Commun.* **17** 1374

[33] Srinivas B, Kumar B G and Muralidharan K 2015 *J. Mol. Cat. A: Chem.* **410** 8

[34] Chaki S H, Deshpande M P, Chaudhary M D and Mahato K S 2013 *Adv. Sci. Eng. Med.* **5** 285

[35] Bharathi B, Thanikaikarasan P, Kollu P V, Chandrasekar K, Sankaranarayanan S and Shajan S 2014 *J. Mater. Sci.: Mater. Electron* **25** 5338

[36] Mahmood K, Sankar S B and Suk J H 2014 *Nanoscale* **6** 9127

[37] Patil S S, Bagade C S, Joshi M P, Kharade S D, Khot K K V, Mali S S *et al* 2018 *J. Mater. Sci.: Mater. Electron.* **29** 19322

[38] Abdelhady A L, Karthik Ramasamy K, Malik M Z, Paul O B, Haigh S J and Raftery J 2011 *J. Mater. Chem.* **21** 17888

[39] Qin N, Wei W, Huang C and Mi L 2020 *Catalysts* **10** 40

[40] Sahraei R, Noshadi S and Goudarzi A 2015 *RSC Adv.* **5** 77354

[41] Mageshwari K, Mali S S, Hemalatha T, Sathyamoorthy R and Patil P S 2011 *Prog. Solid State Chem.* **39** 108

[42] Goudarzi A, Namghi A D and Ha C S 2014 *RSC Adv.* **4** 59764

[43] Chaki S H, Deshpande M P and Jiten P 2014 *Thin Solid Films* **550** 291

[44] Soltani N, Saion E, Mahmood Mat Yunus W, Navasery M, Bahmanrokh G, Erfani M *et al* 2013 *Sol. Energy* **97** 147

[45] Yang T H, De Huang L, Harn Y W, Lin C C, Chang J K, Wu C I *et al* 2013 *Small* **9** 3169

[46] Adhikari S, Sarkar D and Madras G 2017 *ACS Omega* **2** 4009

[47] Chong M N, Jin B, Chow C W K and Saint C 2010 *Water Res.* **44** 2997

[48] Mi L, Wei W, Zheng Z, Gao Y, Liu Y, Chen W *et al* 2013 *Nanoscale* **5** 6589

[49] Bramhaiah K, Bhuyan R, Mandal S, Kar S, Prabhu R, John N S *et al* 2021 *J. Phys. Chem. C* **125** 4299

[50] Raj S I and Jaiswal A 2021 *J. Photochem. Photobiol. A: Chem.* **410** 113158

[51] Basu M, Sinha A K, Pradhan M, Sarkar S, Negishi Y and Pal Govind T 2010 *Environ. Sci. Technol.* **44** 6313

[52] Kaiser A B, Cristina G N, Sundaram R S, Burghard M and Kern K 2009 *Nano Lett.* **9** 1787

[53] Gan Z, Wu X, Meng M, Zhu X, Yang L and Chu P K 2014 *ACS Nano* **8** 9304

[54] Wang F, Huang Y, Chai Z, Zeng M, Li Q, Wang Y *et al* 2015 *Chem. Sci.* **7** 6887

[55] Zhang T, Oyama T, Aoshima A, Hidaka H, Zhao J and Serpone N 2001 *J. Photochem. Photobiol. A Chem.* **140** 163

[56] Timko B P, Dvir T and Kohane D S 2010 *Adv. Mater.* **22** 4925